

Quantum trajectories of dissipative time crystals

Albert Cabot ^{1,*}, Leah Sophie Muhle,¹ Federico Carollo ¹ and Igor Lesanovsky ^{1,2,3}

¹*Institut für Theoretische Physik, Eberhard Karls Universität Tübingen, Auf der Morgenstelle 14, 72076 Tübingen, Germany*

²*School of Physics, Astronomy, University of Nottingham, Nottingham NG7 2RD, England, United Kingdom*

³*Centre for the Mathematics and Theoretical Physics of Quantum Non-Equilibrium Systems, University of Nottingham, Nottingham NG7 2RD, England, United Kingdom*



(Received 10 January 2023; revised 30 March 2023; accepted 20 September 2023; published 17 October 2023)

We explore the boundary time-crystal transition at the level of quantum trajectories which result from continuous monitoring. This Letter is motivated by recent experiments [G. Ferioli, A. Glicenstein, I. Ferrier-Barbut, and A. Browaeys, *Nat. Phys.* **19**, 1345 (2023)] realizing this many-body system and which allow one in principle to gain *in situ* information on its nonequilibrium dynamics. We find that the photon count signal as well as the homodyne current allow one to identify and characterize critical behavior at the time-crystal phase transition. In the time-crystal phase these quantities display persistent oscillations, resolvable in finite systems and in individual realizations. At the transition point the dynamics of the emission signals feature intermittent strong fluctuations, which can be understood through a simple nonlinear phase model. We furthermore show that the time-integrated homodyne current can serve as a useful dynamical order parameter. From this perspective the time crystal can be viewed as a state of matter in which different oscillation patterns coexist.

DOI: [10.1103/PhysRevA.108.L041303](https://doi.org/10.1103/PhysRevA.108.L041303)

The interplay between driving and dissipation can stabilize genuine nonequilibrium phases of interacting quantum systems [1–5]. A manifestation currently receiving significant attention is time crystals [6], which are many-body phases that break time-translation symmetry. Time crystals were initially considered in closed Hamiltonian systems [7]. However, a series of no-go theorems showed that these cannot emerge as the equilibrium state of short-ranged interacting systems [8–13]. While time crystals can still emerge in the presence of long-range interacting Hamiltonians [14], research has generally focused on nonequilibrium scenarios, such as driven Hamiltonian systems [6,15–19] and driven-dissipative systems [6,18,20]. These crystalline structures in time can emerge as a consequence of different mechanisms but they all manifest in stable oscillatory asymptotic regimes [6,18,19]. This means that at long times observables display a periodicity in time that breaks either the discrete (i.e., by displaying a subharmonic response) [15–17,21–31] or the continuous [20,32–40] time-translation symmetry of the dynamical generator. A setting in which such nonequilibrium dynamics can be studied is constituted by atomic ensembles interfaced with optical cavities [41] or photonic structures [42]. In these systems spatial self-organization and steady-state superradiance [43–46], synchronization [47–50], as well as time-crystal oscillations [27,29,30,32,33,51,52] have been reported. Even in free space, i.e., without enhancing collective effects through a cavity, long-time oscillatory dynamics can be supported within dense atomic ensembles. This has been discussed in early theoretical studies on cooperative resonance fluorescence—see, e.g., [53–56]—long before the concept of time crystals was established. In these dense gases, coherently driven (two-

level) atoms are subject to collective dissipation [57], which ultimately stabilizes time-periodic solutions. This conceptually simple system, which in the current terminology would be referred to as a (dissipative) boundary time crystal [20,33,35], was recently realized in an experiment [58]. This achievement opens up a new perspective for exploring and characterizing the time-crystal transition in a dissipative setting. This is owed to the fact that an open system allows one to extract *in situ* information on the quantum many-body dynamics.

In this Letter, we show how the transition and the concomitant critical behavior manifest at the level of quantum trajectories which result from continuous monitoring. We consider two different measurement schemes which yield qualitatively distinct types of quantum trajectories: the record of emitted photons and the quadrature (photocurrent) of the output light field. Both the quantum jump trajectories of photon counting as well as the homodyne (diffusive) trajectories of the photocurrent display clear signatures of the time-crystal phase transition. We show how these experimentally accessible quantities allow one to identify the critical point. Here the trajectories show a peculiar dynamical behavior with small drifts being interspersed with large jumps, and the average time between jumps follows a characteristic power law. Furthermore, we demonstrate that a convenient method for characterizing the time-crystal phase transition is the use of dynamical order parameters, such as the time-integrated photocurrent. When coupling to the appropriate quadrature, the photocurrent shows highly intermittent behavior in the time-crystal phase. This peculiarity can be interpreted as dynamical coexistence between various time-crystalline, i.e., periodic, solutions.

Time-crystal phase transition in the thermodynamic limit. The model we consider here consists of N two-level atoms with coherent resonant driving and collective dissipation. Its dynamics is described by a Markovian master equation

*Corresponding author: albert.cabot@itp.uni-tuebingen.de

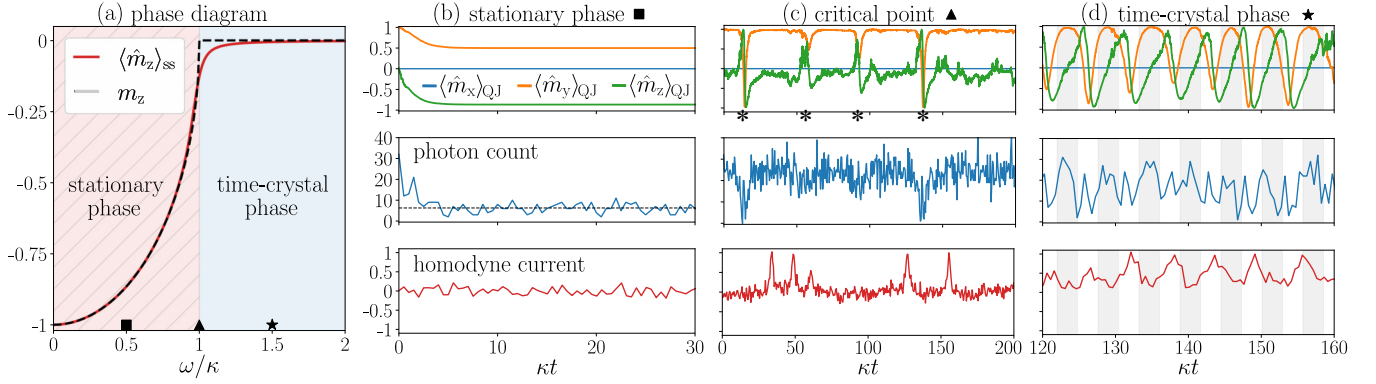


FIG. 1. Signatures of the dynamical regimes in individual realizations. (a) Stationary value of the z component of the magnetization, m_z , for $N = 100$ (red solid line) and time-averaged mean-field solution for $\mathcal{M} = 0$ (black dashed line). At $\omega/\kappa = 0.5$ (■) and $\omega/\kappa = 1.5$ (★) the system is in the stationary phase and the time-crystal phase, respectively. At the critical point $\omega/\kappa = 1$ (▲) the phase transition takes place. (b)–(d) Representative quantum trajectories for the magnetization components (top), the photon count (middle), and the homodyne current (bottom). The photon count trajectories are displayed with a bin size $\kappa\Delta t = 0.5$, while the homodyne current is averaged over a sliding time window of $\kappa\Delta t = 0.5$ and rescaled by $1/\sqrt{2N}$. In all cases $N = 100$ and the initial condition corresponds to a spin coherent state as defined by $|\theta, \phi\rangle = \exp[i\theta(\hat{J}_x \sin \phi - \hat{J}_y \cos \phi)]|J, J\rangle$ ($\theta \in [0, \pi]$, $\phi \in [0, 2\pi]$) [59] with $\theta = \pi/2$ and $\phi = \pi/2$.

governing the time evolution of the density matrix $\hat{\rho}$ as ($\hbar=1$)

$$\partial_t \hat{\rho} = \mathcal{L} \hat{\rho} = -i\omega[\hat{J}_x, \hat{\rho}] + \frac{\kappa}{N}(2\hat{J}_- \hat{\rho} \hat{J}_+ - \hat{J}_+ \hat{J}_- \hat{\rho} - \hat{\rho} \hat{J}_+ \hat{J}_-). \quad (1)$$

Here ω is the Rabi frequency, which parametrizes the coupling strength between the atoms and the laser, and $2\kappa/N$ is the collective atomic decay rate. Note that the latter scales with $1/N$, which is necessary for obtaining a well-defined thermodynamic limit. The master equation solely depends on collective spin operators defined as $\hat{J}_\alpha = \frac{1}{2} \sum_{j=1}^N \hat{\sigma}_\alpha^{(j)}$ ($\alpha = x, y, z$), with $\hat{\sigma}_\alpha^{(j)}$ being the Pauli matrices and $\hat{J}_\pm = \hat{J}_x \pm i\hat{J}_y$. As shown in [20,35,56,60] it is convenient to introduce the magnetization vector with components $\hat{m}_\alpha = \hat{J}_\alpha/(N/2)$. In the thermodynamic limit ($N \rightarrow \infty$) the dynamics of the expectation values $m_\alpha = \langle \hat{m}_\alpha \rangle$ is exactly governed by the mean-field equations $\dot{m}_x = \kappa m_x m_z$, $\dot{m}_y = -\omega m_z + \kappa m_y m_z$, and $\dot{m}_z = \omega m_y - \kappa(m_x^2 + m_y^2)$. The ensuing dynamics features two conserved quantities, which are the total angular momentum $j^2 = m_x^2 + m_y^2 + m_z^2$ and the quantity $\mathcal{M} = m_x/(m_y - \omega/\kappa)$ (we will focus throughout on the case $j^2 = 1$, $\mathcal{M} = 0$).

The model undergoes a nonequilibrium phase transition at the critical ratio $\omega/\kappa = 1$. Below this critical point, the system approaches a unique stable stationary fixed point. Above the critical point, $\omega/\kappa > 1$, it displays a continuous family of nonisolated closed orbits covering the whole Bloch sphere [20,55,56]. Each orbit is associated with a value of the conserved quantity \mathcal{M} . The emergence of this nonequilibrium transition for finite particle number N is signaled by a sharp crossover of the stationary value of the z component of the magnetization, $\langle \hat{m}_z \rangle_{ss}$, at $\omega/\kappa = 1$ [see Fig. 1(a)].

Time-crystal phase transition in finite systems. The master equation (1) describes the average evolution of an open system in terms of its density matrix $\hat{\rho}$. In an experiment, however, one observes stochastic realizations of the open systems dynamics—the so-called quantum trajectories. Averaging over these individual realizations yields the density matrix. To be specific, let us consider the dynamics of the

magnetization components in the stationary phase, which are shown in the top panel of Fig. 1(b). These curves are obtained by a so-called quantum jump unraveling [61] (see also Supplemental Material [62]) of Eq. (1). In the stationary phase all magnetization components rapidly approach a constant value. Moreover, in spite of representing a single realization, they hardly display any fluctuations. The reason is that the stationary state is almost pure and an eigenstate of the jump operator, i.e., it satisfies to a very good approximation the relation

$$\hat{\rho}_{ss} \approx |\beta\rangle\langle\beta|, \quad \hat{J}_-|\beta\rangle \approx -i\beta|\beta\rangle \quad (2)$$

with $\beta = \omega N/(2\kappa)$. In fact, when approaching the thermodynamic limit the system features such pure stationary state in the entire interval $0 \leq \omega/\kappa \leq 1$ (see [62]).

The trajectories shown in the top panel of Fig. 1(b) are not directly observable in experiment, as they entail the calculation of quantum expectation values $\langle \hat{m}_\alpha \rangle_{\text{QJ}}$ with the instantaneous wave function. By the nature of a quantum measurement such quantity cannot be obtained in a single shot. What is instead experimentally accessible—e.g., in the experiment presented in Ref. [58]—is the time record of emitted photons, which is shown in the middle panel of Fig. 1(b). Note that this record corresponds to the same trajectory shown in the top row, which is also the case for Figs. 1(c) and 1(d). The rapid approach to stationarity is also visible here albeit fluctuations around the average value of the photon count (dashed black line) are clearly visible. Instead of counting photons one can monitor the so-called x quadrature of the emitted light using a homodyne detection scheme [61] (see [62]), which measures the homodyne current $I_x(t) = \sqrt{2\kappa N}(\hat{m}_x(t))_{\text{H}} + dW(t)/dt$. This observable is proportional to the instantaneous x magnetization in the homodyne unraveling, indicated by the subscript H, plus the derivative of a random (Wiener) process $W(t)$ [61,62]. Removing this noise, via the application of a sliding average over the time windows $\kappa\Delta t = 0.5$, yields the trajectories shown in the bottom row of Figs. 1(b)–1(d).

Let us now turn to Fig. 1(c), which shows the quantum trajectories at the critical point $\omega/\kappa = 1$. Here the dynamics is strikingly different. All observables display a behavior in which periods of time, in which the quantum trajectories feature small fluctuations and drifts, are interspersed with sudden large fluctuations (marked with *). This peculiar behavior, signatures of which are also found in the photon count and—more clearly—in the homodyne current, will be further analyzed below. We will find that the mean time between two consecutive large fluctuation events follows a power law which is characteristic for critical phenomena.

In the time-crystal phase the quantum trajectories of the magnetization exhibit nondecaying oscillatory behavior, as can be seen in Fig. 1(d). Noise due to quantum jumps leads, however, to the relative dephasing of different trajectories, so that the average state displays exponentially damped oscillations [20]. This dephasing is observable in the oscillations of the magnetization when comparing them with the shadowed background that alternates in time intervals that are half the mean-field period. Note that the larger the number of particles the weaker the dephasing effect until noiseless oscillations are achieved in the mean-field limit [20,33,35]. Interestingly, also the photon count signal displays noisy but pronounced oscillations and thus allows for an *in situ* detection of the time-crystal phase. In fact, the Fourier transform of the counting signal displays a peak at the mean-field frequency [62]. This peak becomes better resolved increasing system size as time-crystal oscillations become less noisy [62]. The time-crystal oscillations are also resolved in the (time-averaged) homodyne current shown in the bottom panel of Fig. 1(d).

Dynamics near the critical point. In Fig. 1(c) we have shown that the dynamics of the quantum trajectories at the critical point is rather peculiar. To understand this behavior we return to the mean-field equations for the magnetization and augment the corresponding equations with Gaussian noise. We consider the case in which $m_x(0) = 0$, which implies that the conserved quantity \mathcal{M} takes the value zero. Notice that this is the most relevant case for photocounting trajectories, as for long times the trajectories display a “fluctuationless” zero x component independently of the initial condition (see Fig. 1 and [62]). Defining the phase variable φ via $m_y^\varphi = \sin \varphi$ and $m_z^\varphi = \cos \varphi$ leads to the following equation of motion:

$$\dot{\varphi}(t) = -\omega + \kappa \sin \varphi(t) + \xi(t). \quad (3)$$

Here the Gaussian noise $\xi(t)$ is introduced to model the effect of finite- N fluctuations and is characterized by the average value $\langle \xi(t) \rangle = 0$ and the correlation function $\langle \xi(t)\xi(t') \rangle = \frac{2\kappa}{N} \delta(t - t')$. The prefactor of the latter is chosen such that the noise vanishes in the thermodynamic limit.

The phase portrait of the deterministic part of this equation is shown in Fig. 2(a). Below the critical point there are one stable and one unstable fixed point which approach each other when ω increases. They coalesce and annihilate when the critical point, $\omega/\kappa = 1$, is reached, for which the solution of the deterministic equation becomes a limit cycle. This time-periodic solution is nonharmonic, as the velocity of the phase evolution depends on φ . In particular, around $\varphi \approx \pi/2$ this velocity decreases and becomes zero when the critical point is approached from above. This means in turn that the period of the oscillation diverges [67]. The proximity of the

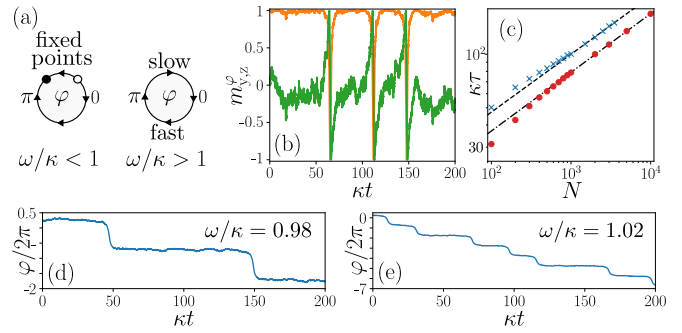


FIG. 2. Dynamics near the critical point. (a) Flow of the phase equation below and above the critical point, where \bullet (\circ) denotes a (un)stable fixed point (full or empty bullet point). (b) Single realization of Eq. (3) with initial conditions $\varphi = \pi/2$, $N = 200$, and $\omega/\kappa = 1$. (c) Average time between large fluctuations for $\omega/\kappa = 1$ and varying N . Red circles correspond to the classical model fitted by $\kappa\tau \propto N^{0.330}$ (black dashed-dotted line). Blue crosses correspond to the quantum jump process fitted by $\kappa\tau \propto N^{0.326}$ (dashed black line). Error bars for each point are smaller than the symbols (see [62] for more details). (d), (e) Classical phase dynamics for two different frequencies.

two fixed points slightly below criticality and the slowdown of the dynamics near $\varphi \approx \pi/2$ explain the large fluctuations observed in Fig. 2(b): slightly below the critical point, the noise occasionally allows the system to reach the unstable fixed point. After that φ may immediately complete a full cycle in clockwise direction [Fig. 2(d)], manifesting as a large fluctuation $m_{y,z}^\varphi$. On the other hand, slightly above the critical point, the noise can allow φ to escape the region with small velocity, so that it undergoes afterwards a fast revolution, which also manifests as a large fluctuation $m_{y,z}^\varphi$ [see Fig. 2(e)]. The average time τ between such large fluctuations as a function of N is shown in Fig. 2(c) (red circles). As it can be seen, it obeys a power law, $\tau \propto N^{0.330}$, which is characteristic for critical phenomena [68]. The same power law (within a reasonable margin of error) is observed for the average time between large fluctuations in the time-crystal trajectories (see [62] for details). Therefore the phase model (3) captures the phenomenology observed in quantum jump trajectories, providing insights on the critical dynamics observed in Fig. 1(c).

Dynamical coexistence of oscillation patterns. In the following, we will show that in the time-crystal phase the dynamics is composed of different oscillatory patterns which dynamically coexist. This means that the quantum state features a given periodic solution for a long time window but then eventually jumps at a random time into another one. This persistent jumping is related to a first-order dynamical phase transition [69–71]. To understand this, one has to keep in mind that, for the system in the thermodynamic limit, the breaking of the time-translation symmetry in the time-crystal regime results in the stabilization of several different oscillatory solutions, which are “approached” according to the specific initial condition for the system state. However, when considering a finite system (subject to quantum fluctuations), the (long-time) state of the system is actually time-translation symmetric, indicating that the latter must consist of the “sum” of the different oscillatory patterns [56]. This *statistical*

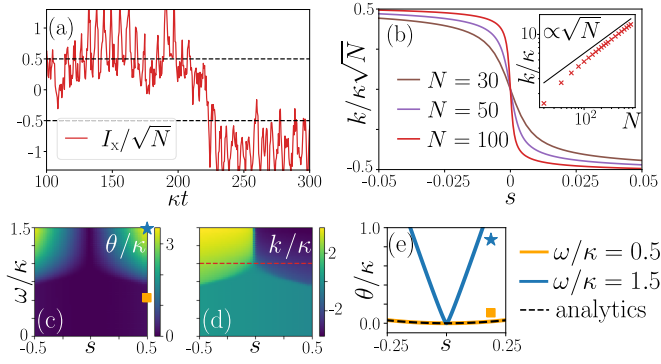


FIG. 3. Dynamical order parameter. (a) Rescaled homodyne current for $\omega/\kappa = 1.5$, $N = 100$, and an initial condition of a coherent state with $\theta = \pi/2$ and $\phi = \pi/2$. (b) Rescaled activity $k(s)$ for various system sizes and $\omega/\kappa = 1.5$. Inset: Scaling of the activity at $s = -0.025$ and $\omega/\kappa = 1.5$ with system size. (c), (d) Color maps for the scaled cumulant generating function $\theta(s)$ and the activity $k(s)$ for the homodyne current. (e) Scaled cumulant generating function $\theta(s)$ for two different values of ω/k , one above and one below the critical point.

mixture of oscillations is realized by the coexistence of all the possible oscillatory patterns in single homodyne trajectories.

The above phenomenology is clearly displayed by single dynamical realizations of the homodyne current—in the time-crystal regime—when looking at sufficiently large timescales as shown in Fig. 3(a). Here, the homodyne current shows oscillations which switch from a pattern with a positive average value to a pattern with a negative one. On average the overall current must average to zero due to the expected value $\langle \hat{m}_x \rangle_{ss} = 0$. One way to describe the emergence of this coexistence regime is achieved by using a “thermodynamic formalism” for the full statistical characterization of the probability density $p_K(t)$ of observing a given value of the time integrated homodyne current $K_t = \int_0^t dt' I_x(t')$. Such characterization can be obtained via the moment generating function $Z(s) = \int dK e^{-sK} p_K(t)$. For large times t , this function behaves as $Z(s) \approx e^{t\theta(s)}$, where $\theta(s)$ is the so-called scaled cumulant generating function for K_t . This function can be computed as the largest real eigenvalue of the tilted generator [69,72,73]:

$$\mathcal{L}_s \hat{\rho} = \mathcal{L} \hat{\rho} - s \sqrt{\frac{2\kappa}{N}} (\hat{J}_- \hat{\rho} + \hat{\rho} \hat{J}_+) + \frac{s^2}{2} \hat{\rho}. \quad (4)$$

For instance, the average value of K_t is given by the first derivative $k(s) = -\partial_s \theta(s)$, calculated for $s = 0$. When considered as a function of s , the scaled cumulant generating function $\theta(s)$ plays the role of a dynamical free energy, while the activity $k(s)$ can be regarded as an order parameter which can signal emergent dynamical behavior in quantum trajectories [69,70,74,75]. This is for instance evident in Fig. 3(b), where we plot the function $k(s)$ rescaled by $1/\sqrt{N}$. The activity $k(0)$ provides the average value of the time-integrated current in the typical trajectories, which is zero since there appear oscillatory patterns which are symmetric around $\langle \hat{m}_x \rangle_{ss} = 0$. Around $s = 0$, we see that the activity

displays a rapid crossover from a phase with positive homodyne current to a phase with negative homodyne current. Such a crossover tends to approach a discontinuous transition when N is increased. As for equilibrium phase transitions, this (almost) discontinuous behavior signals that in the typical trajectories, i.e., at $s = 0$, there emerges coexistence of the two different phases, which here takes place in single stochastic realizations of the dynamics. It is possible to look at the dynamics for $s \neq 0$ (see [62]). Here, the coexistence behavior is resolved by the parameter s , which plays the role of a biasing field, and single trajectories show a unique stable oscillatory pattern for sufficiently large $|s|$.

Such a critical behavior of the functions $\theta(s)$ and $k(s)$ disappears below the critical point, as shown in Figs. 3(c) and 3(d). In this case, the system approaches a unique stable stationary state characterized by vanishing instantaneous value of the average homodyne current and by small fluctuations. In particular, exploiting the approximate relation in Eq. (2), we can obtain the analytical expression $\theta(s) \approx s^2/2$ that we display in Fig. 3(e) together with the numerical result. We notice that this expression for $\theta(s)$ comes exclusively from the last term in the tilted generator in Eq. (4), suggesting that the output homodyne current is essentially a pure white noise. This is in contrast with what happens above the critical point [see Fig. 3(e)], where $\theta(s)$ becomes singular.

Summary and conclusions. Motivated by recent experimental progress, we analyzed signatures of a time-crystal phase transition in experimentally accessible quantum jump and homodyne trajectories. We illustrated how stationary and oscillatory phases manifest in these trajectories and unveiled peculiarities of the dynamics at the critical point. We found the time-crystal phase to display persistent oscillations in individual realizations and for *finite* systems, thus emerging in the presence of significant fluctuations beyond the mean-field limit. At criticality, we disclosed the occurrence of large fluctuations and we could show the average time between them to display a power-law scaling with system size. We moreover showed that the time-integrated photocurrent can serve as a dynamical order parameter for the time-crystal phase transition. From this perspective the time-crystal phase can be regarded as a phase in which many oscillatory patterns coexist. This dynamical phase coexistence manifests in strongly intermittent behavior of the photocurrent. It would be interesting to understand, whether the dynamical transition may be useful as a resource for quantum enhanced metrology, as discussed in [76].

Acknowledgments. We are grateful for financing from the Baden-Württemberg Stiftung through Project No. BWST_ISF2019-23. We also acknowledge funding from the Deutsche Forschungsgemeinschaft under Project No. 435696605 and through the Research Unit FOR 5413/1, Grant No. 465199066. This project has also received funding from the European Unions Horizon Europe research and innovation program under Grant No. 101046968 (BRISQ). F.C. is indebted to the Baden-Württemberg Stiftung for financial support by the Eliteprogramme for Postdocs. We acknowledge the use of the QUTIP PYTHON library [77,78] for performing some of the computer simulations of this Letter.

- [1] S. Diehl, A. Micheli, A. Kantian, B. Kraus, H. Büchler, and P. Zoller, *Nat. Phys.* **4**, 878 (2008).
- [2] S. Diehl, A. Tomadin, A. Micheli, R. Fazio, and P. Zoller, *Phys. Rev. Lett.* **105**, 015702 (2010).
- [3] T. E. Lee, S. Gopalakrishnan, and M. D. Lukin, *Phys. Rev. Lett.* **110**, 257204 (2013).
- [4] J. Jin, D. Rossini, R. Fazio, M. Leib, and M. J. Hartmann, *Phys. Rev. Lett.* **110**, 163605 (2013).
- [5] M. Marcuzzi, E. Levi, S. Diehl, J. P. Garrahan, and I. Lesanovsky, *Phys. Rev. Lett.* **113**, 210401 (2014).
- [6] D. V. Else, C. Monroe, C. Nayak, and N. Y. Yao, *Annu. Rev. Condens. Matter Phys.* **11**, 467 (2020).
- [7] F. Wilczek, *Phys. Rev. Lett.* **109**, 160401 (2012).
- [8] P. Bruno, *Phys. Rev. Lett.* **110**, 118901 (2013).
- [9] P. Bruno, *Phys. Rev. Lett.* **111**, 070402 (2013).
- [10] P. Nozières, *Europhys. Lett.* **103**, 57008 (2013).
- [11] H. Watanabe and M. Oshikawa, *Phys. Rev. Lett.* **114**, 251603 (2015).
- [12] P. Öhberg and E. M. Wright, *Phys. Rev. Lett.* **123**, 250402 (2019).
- [13] A. Syrwid, A. Kosior, and K. Sacha, *Phys. Rev. Res.* **2**, 032038(R) (2020).
- [14] V. K. Kozin and O. Kyriienko, *Phys. Rev. Lett.* **123**, 210602 (2019).
- [15] V. Khemani, A. Lazarides, R. Moessner, and S. L. Sondhi, *Phys. Rev. Lett.* **116**, 250401 (2016).
- [16] D. V. Else, B. Bauer, and C. Nayak, *Phys. Rev. Lett.* **117**, 090402 (2016).
- [17] N. Y. Yao, A. C. Potter, I.-D. Potirniche, and A. Vishwanath, *Phys. Rev. Lett.* **118**, 030401 (2017).
- [18] K. Sacha and J. Zakrzewski, *Rep. Prog. Phys.* **81**, 016401 (2018).
- [19] M. P. Zaletel, M. Lukin, C. Monroe, C. Nayak, F. Wilczek, and N. Y. Yao, *Rev. Mod. Phys.* **95**, 031001 (2023).
- [20] F. Iemini, A. Russomanno, J. Keeling, M. Schirò, M. Dalmonte, and R. Fazio, *Phys. Rev. Lett.* **121**, 035301 (2018).
- [21] A. Pizzi, A. Nunnenkamp, and J. Knolle, *Phys. Rev. Lett.* **127**, 140602 (2021).
- [22] Z. Gong, R. Hamazaki, and M. Ueda, *Phys. Rev. Lett.* **120**, 040404 (2018).
- [23] R. R. W. Wang, B. Xing, G. G. Carlo, and D. Poletti, *Phys. Rev. E* **97**, 020202(R) (2018).
- [24] F. M. Gambetta, F. Carollo, M. Marcuzzi, J. P. Garrahan, and I. Lesanovsky, *Phys. Rev. Lett.* **122**, 015701 (2019).
- [25] A. Lazarides, S. Roy, F. Piazza, and R. Moessner, *Phys. Rev. Res.* **2**, 022002(R) (2020).
- [26] A. Riera-Campenya, M. Moreno-Cardoner, and A. Sanpera, *Quantum* **4**, 270 (2020).
- [27] B. Zhu, J. Marino, N. Y. Yao, M. D. Lukin, and E. A. Demler, *New J. Phys.* **21**, 073028 (2019).
- [28] K. Chinzei and T. N. Ikeda, *Phys. Rev. Lett.* **125**, 060601 (2020).
- [29] H. Keßler, P. Kongkhambut, C. Georges, L. Mathey, J. G. Cosme, and A. Hemmerich, *Phys. Rev. Lett.* **127**, 043602 (2021).
- [30] R. J. L. Tuquero, J. Skulte, L. Mathey, and J. G. Cosme, *Phys. Rev. A* **105**, 043311 (2022).
- [31] S. Sarkar and Y. Dubi, *Commun. Phys.* **5**, 155 (2022).
- [32] K. Tucker, B. Zhu, R. J. Lewis-Swan, J. Marino, F. Jimenez, J. G. Restrepo, and A. M. Rey, *New J. Phys.* **20**, 123003 (2018).
- [33] G. Buonaiuto, F. Carollo, B. Olmos, and I. Lesanovsky, *Phys. Rev. Lett.* **127**, 133601 (2021).
- [34] C. Lledó and M. H. Szymaska, *New J. Phys.* **22**, 075002 (2020).
- [35] F. Carollo and I. Lesanovsky, *Phys. Rev. A* **105**, L040202 (2022).
- [36] K. Seibold, R. Rota, and V. Savona, *Phys. Rev. A* **101**, 033839 (2020).
- [37] B. Buča and D. Jaksch, *Phys. Rev. Lett.* **123**, 260401 (2019).
- [38] B. Buča, J. Tindall, and D. Jaksch, *Nat. Commun.* **10**, 1730 (2019).
- [39] C. Booker, B. Buča, and D. Jaksch, *New J. Phys.* **22**, 085007 (2020).
- [40] M. Hajdušek, P. Solanki, R. Fazio, and S. Vinjanampathy, *Phys. Rev. Lett.* **128**, 080603 (2022).
- [41] H. Ritsch, P. Domokos, F. Brennecke, and T. Esslinger, *Rev. Mod. Phys.* **85**, 553 (2013).
- [42] D. E. Chang, J. S. Douglas, A. González-Tudela, C.-L. Hung, and H. J. Kimble, *Rev. Mod. Phys.* **90**, 031002 (2018).
- [43] P. Domokos and H. Ritsch, *Phys. Rev. Lett.* **89**, 253003 (2002).
- [44] D. Meiser, J. Ye, D. R. Carlson, and M. J. Holland, *Phys. Rev. Lett.* **102**, 163601 (2009).
- [45] J. G. Bohnet, Z. Chen, J. M. Weiner, D. Meiser, M. J. Holland, and J. K. Thompson, *Nature (London)* **484**, 78 (2012).
- [46] M. A. Norcia and J. K. Thompson, *Phys. Rev. X* **6**, 011025 (2016).
- [47] M. Xu, D. A. Tieri, E. C. Fine, J. K. Thompson, and M. J. Holland, *Phys. Rev. Lett.* **113**, 154101 (2014).
- [48] B. Zhu, J. Schachenmayer, M. Xu, F. Herrera, J. G. Restrepo, M. J. Holland, and A. M. Rey, *New J. Phys.* **17**, 083063 (2015).
- [49] B. Bellomo, G. L. Giorgi, G. M. Palma, and R. Zambrini, *Phys. Rev. A* **95**, 043807 (2017).
- [50] A. Cabot, G. L. Giorgi, F. Galve, and R. Zambrini, *Phys. Rev. Lett.* **123**, 023604 (2019).
- [51] H. Keßler, J. G. Cosme, C. Georges, L. Mathey, and A. Hemmerich, *New J. Phys.* **22**, 085002 (2020).
- [52] P. Kongkhambut, J. Skulte, L. Mathey, J. G. Cosme, A. Hemmerich, and H. Keßler, *Science* **377**, 670 (2022).
- [53] G. S. Agarwal, A. C. Brown, L. M. Narducci, and G. Vetri, *Phys. Rev. A* **15**, 1613 (1977).
- [54] L. M. Narducci, D. H. Feng, R. Gilmore, and G. S. Agarwal, *Phys. Rev. A* **18**, 1571 (1978).
- [55] P. Drummond and H. Carmichael, *Opt. Commun.* **27**, 160 (1978).
- [56] H. J. Carmichael, *J. Phys. B* **13**, 3551 (1980).
- [57] R. H. Dicke, *Phys. Rev.* **93**, 99 (1954).
- [58] G. Ferioli, A. Glicenstein, I. Ferrier-Barbut, and A. Browaeys, *Nature Physics* **19**, 1345 (2023).
- [59] J. Ma, X. Wang, C. Sun, and F. Nori, *Phys. Rep.* **509**, 89 (2011).
- [60] F. Benatti, F. Carollo, R. Floreanini, and H. Narnhofer, *J. Phys. A* **51**, 325001 (2018).
- [61] H. M. Wiseman and G. J. Milburn, *Quantum Measurement and Control* (Cambridge University Press, New York, 2009).
- [62] See Supplemental Material at <http://link.aps.org/supplemental/10.1103/PhysRevA.108.L041303> for details, which includes Refs. [63–66].
- [63] C. Gardiner and P. Zoller, *Quantum Noise: A Handbook of Markovian and Non-Markovian Quantum Stochastic Methods with Applications to Quantum Optics* (Springer, New York, 2004).

- [64] J. Hannukainen and J. Larson, *Phys. Rev. A* **98**, 042113 (2018).
- [65] J. Roberts and G. Quispel, *Phys. Rep.* **216**, 63 (1992).
- [66] P. Fornasini, *The Uncertainty in Physical Measurements: An Introduction to Data Analysis in the Physics Laboratory* (Springer, New York, 2008).
- [67] S. H. Strogatz, *Nonlinear Dynamics and Chaos: With Applications to Physics, Biology, Chemistry, and Engineering* (CRC Press, Boca Raton, FL, 2018).
- [68] N. Goldenfeld, *Lectures on Phase Transitions and the Renormalization Group* (CRC Press, Boca Raton, FL, 2018).
- [69] J. P. Garrahan and I. Lesanovsky, *Phys. Rev. Lett.* **104**, 160601 (2010).
- [70] C. Ates, B. Olmos, J. P. Garrahan, and I. Lesanovsky, *Phys. Rev. A* **85**, 043620 (2012).
- [71] F. Carollo, J. P. Garrahan, I. Lesanovsky, and C. Pérez-Espigares, *Phys. Rev. A* **98**, 010103(R) (2018).
- [72] J. M. Hickey, S. Genway, I. Lesanovsky, and J. P. Garrahan, *Phys. Rev. A* **86**, 063824 (2012).
- [73] F. Carollo, J. P. Garrahan, and R. L. Jack, *J. Stat. Phys.* **184**, 13 (2021).
- [74] S. Genway, J. P. Garrahan, I. Lesanovsky, and A. D. Armour, *Phys. Rev. E* **85**, 051122 (2012).
- [75] I. Lesanovsky, M. van Horssen, M. Guță, and J. P. Garrahan, *Phys. Rev. Lett.* **110**, 150401 (2013).
- [76] K. Macieszczak, M. Guță, I. Lesanovsky, and J. P. Garrahan, *Phys. Rev. A* **93**, 022103 (2016).
- [77] J. Johansson, P. Nation, and F. Nori, *Comput. Phys. Commun.* **183**, 1760 (2012).
- [78] J. Johansson, P. Nation, and F. Nori, *Comput. Phys. Commun.* **184**, 1234 (2013).